

Article

Dual Phase Lock-In Amplifier with Photovoltaic Modules and Quasi-Invariant Common-Mode Signal

Pavel Baranov *, Ivan Zatonov and Bien Bui Duc

Division for Electronic Engineering, National Research Tomsk Polytechnic University, 30 Lenin Avenue, 634050 Tomsk, Russia; iaz5@tpu.ru (I.Z.); atembui@tpu.ru (B.B.D.)

* Correspondence: bpf@tpu.ru; Tel.: +7-3822701777 (ext. 1685)

Abstract: In measuring small voltage deviations of about 1 μV and lower, it is important to separate useful signals from noise. The measurement of small voltage deviations between the amplitudes of two AC signals in wide frequency and voltage ranges, is performed by using lock-in amplifiers with the differential input as a comparator (null-indicator). The resolution and measurement accuracy of lock-in amplifiers is largely determined by the common-mode rejection ratio in their measuring channel. This work presents a developed differential signal recovery circuit with embedded photovoltaic modules, which allows implementing the dual phase lock-in amplifier with the differential input and quasi-invariant common-mode signal. The obtained metrological parameters of the proposed dual phase analog lock-in amplifier prove its applicability in comparing two signal amplitudes of $10\sqrt{2}$ μV to $10\sqrt{2}$ V in the frequency range of 20 Hz to 100 kHz with a 10 nV resolution. The proposed dual phase analog lock-in amplifier was characterized by a 130 to 185 dB CMRR in the frequency range up to 100 kHz with 20 nV/ $\sqrt{\text{Hz}}$ white noise.

Keywords: lock-in amplifier; common-mode rejection; differential signal; nanovolts resolution



Citation: Baranov, P.; Zatonov, I.; Duc, B.B. Dual Phase Lock-In Amplifier with Photovoltaic Modules and Quasi-Invariant Common-Mode Signal. *Electronics* **2022**, *11*, 1512. <https://doi.org/10.3390/electronics11091512>

Academic Editor: Graziella Scandurra

Received: 24 March 2022

Accepted: 6 May 2022

Published: 9 May 2022

Publisher's Note: MDPI stays neutral with regard to jurisdictional claims in published maps and institutional affiliations.



Copyright: © 2022 by the authors. Licensee MDPI, Basel, Switzerland. This article is an open access article distributed under the terms and conditions of the Creative Commons Attribution (CC BY) license (<https://creativecommons.org/licenses/by/4.0/>).

1. Introduction

In measuring small voltage deviations of about 1 μV and lower, it is important to separate a useful signal from noise. This problem is relevant to the metrological support of measuring transducers, such as inductive voltage dividers [1–4], current shunts [5–7], current transformers, current clamps [8,9] for AC voltage measurements [10–13], vibration measurements of MEMS gyroscopes, accelerometers [14–16] and other sensors [17–24]. The measurement of small voltage deviations between the amplitudes of two AC signals in wide frequency and voltage ranges is performed by using lock-in amplifiers with the differential input as a comparator (null-indicator and null-detector) [25,26].

The resolution and, consequently, measurement accuracy of lock-in amplifiers is largely determined by the common-mode rejection ratio (CMRR) in their measuring channel. The common-mode signal is the half-sum of voltages at measurement inputs of a lock-in amplifier. For example, if two 10 V voltages with 1 nV resolution are compared, the CMRR must be higher than 200 dB.

The best commercially available lock-in amplifiers [27–33] demonstrate a 3–1 nV resolution, which is restricted by the CMRR of 100–120 dB, while its maximum input voltage is not over 1 or 3 V. This is insufficient, for example, metrological support of state-of-the-art measuring instruments, which requires to compare the root-mean-square (RMS) voltages of ≤ 10 V with a resolution to units of nanovolts.

For achievement in the real resolution range of 1–10 nV in the lock-in amplifier with voltages of over 1 V to be compared, it is necessary to achieve a result of transformations fully or partially independent from the common-mode signal, i.e., to implement a quasi-invariant common-mode signal.

This work presents the developed differential signal recovery circuit with embedded photovoltaic modules, which allows implementing the dual phase lock-in amplifier with

the differential input and quasi-invariant common-mode signal. The structure of the paper includes three main sections: about lock-in amplifiers, our differential signal recovery circuit and our developed lock-in amplifier with increased CMRR.

2. Lock-In Amplifiers

Lock-in amplifiers are intended for a low-amplitude useful signal recovery from noise, whose amplitude is hundreds and thousands of times higher. With this purpose, the input signal is amplified and multiplied by a reference signal, the frequency of which equals the frequency of the useful signal. Next, the resulting signal is filtered from high frequencies [34]. This approach is called synchronous demodulation or phase-sensitive detection. The reference signal is generated by the lock-in amplifier or an internal source. The phase-sensitive detection of the reference signal of the specified frequency provides a synchronous measurement on both fundamental and any harmonic frequency of the useful signal [35–42].

Figure 1 illustrates a typical flowchart of a commercially available lock-in amplifier [27–33]. It consists of the instrumentation amplifier IA, programmable gain amplifier PGA, dual channel analog-to-digital converter ADC and digital processing unit.

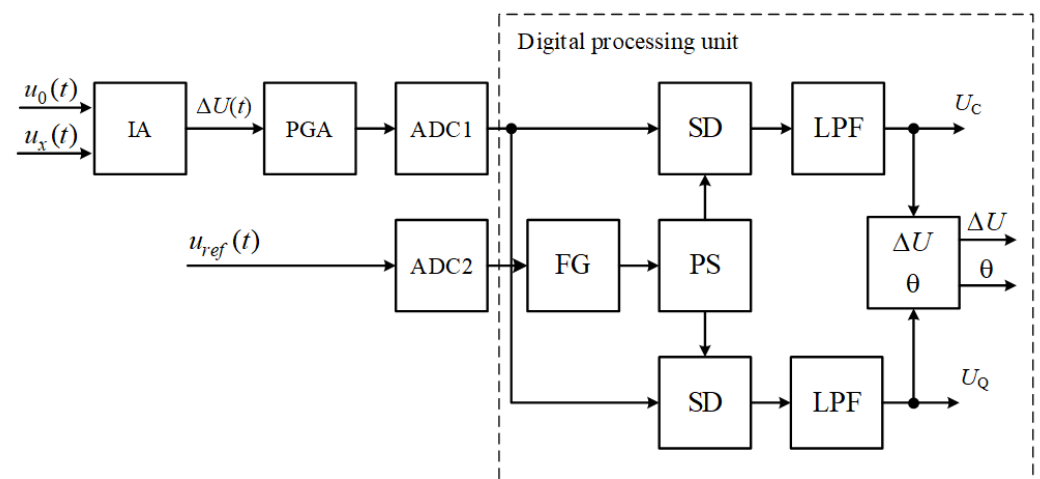


Figure 1. Flowchart of commercially available lock-in amplifier.

Input voltages $u_0(t)$ and $u_x(t)$ are supplied to the IA. The differential voltage $\Delta U(t)$ is amplified by the PGA and processed by the ADC1. The reference voltage $u_{ref}(t)$ is processed by the ADC2. The ADC output signals are processed in the digital processing unit. The latter implements the inner reference frequency generator FG, phase-shifter PS, synchronous detectors SD and low-frequency filters LFF. The signal processing provides the common-mode signal U_C and quadrature signal U_Q of the differential signal. Its module ΔU and phase θ are calculated in the same way.

Table 1 presents specifications for different models of commercially available lock-in amplifiers. Modern lock-in amplifiers are intended for the solutions of different problems, and this determines their high price and standard specifications. Being at the level of typical microcircuits of instrumentation amplifiers, the low common-mode rejection ratio (CMRR) is typical for all commercially available lock-in amplifiers, which makes it impossible to apply standard lock-in amplifiers for the recovery difference of two signals with a high resolution.

As can be seen from Table 1, the real resolution of modern lock-in amplifiers is restricted by 100–120 dB CMRR of the input instrumentation amplifier, while their maximum input voltage does not exceed 1 V, which is insufficient for, for example, metrological support of state-of-the-art measuring instruments, which requires comparing RMS voltages of ≤ 10 V with a resolution in units of nanovolts.

Table 1. Specifications for commercially-available lock-in amplifiers.

Models	Price, USD	Max Input Voltage, V	Resolution, nV	Frequency Range, kHz	CMRR, dB
SR830, Stanford Research Systems	4000	1	2	1×10^{-6} –102	100 (≤ 10 kHz)
SR860, Stanford Research Systems	6495	1	1	1×10^{-6} –500	90 (≤ 1 kHz)
SR865A, Stanford Research Systems	7950	1	1	1×10^{-6} –4000	>90 (≤ 1 kHz)
7260, EG&G Instruments	3250	1	2	1×10^{-6} –250	100 (1 kHz)
LI5640, NF Electronic Instruments	2100	1	2	1×10^{-6} –100	120 (1 kHz)
7265, Signal Recovery	4000	1	2	1×10^{-6} –250	>100 (1 kHz)
7230, Signal Recovery	3390	1	10	1×10^{-6} –120	>100 (1 kHz)
MFLI, Zurich Instruments	5200	3	1	DC–500	100 (1 kHz)

The analysis of errors produced by the main units (see Figure 1) given in our early research [43] shows that the resolution of lock-in amplifiers is mostly affected by the common-mode signal of the input instrumentation amplifier. The development of solutions is, therefore, required to increase the CMRR and develop lock-in amplifiers with quasi-invariant common-mode signal.

3. Differential Signal Recovery

The circuit solutions based on the common-mode signal compensation, data correction of the common-mode signal and voltage follower can be used to increase the CMRR in IA subtraction circuits and to design lock-in amplifiers with a quasi-invariant common-mode signal.

The common-mode signal compensation and correction circuits have significant limitations [44–47] that restrict their practical use in lock-in amplifiers. These limitations include a limited maximum amplitude of input signals owing to a low IA voltage, at least two IAs with identical parameters, additional functional modules with super low-level errors of both the modulus and phase shift transfer factors in a wide frequency range.

The input range can be broadened without the voltage increase of the IA supply voltage, and the common-mode rejection ratio can be, thus, increased via changing the IA supply voltage in sync with changing the input common mode voltage [48]. Figure 2 shows the schematic circuit of the differential signal recovery based on the voltage follower, which utilizes this principle for the CMRR increase.

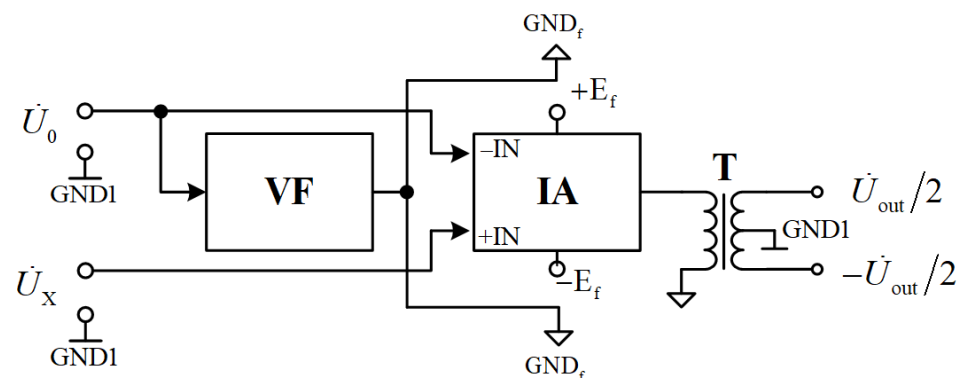


Figure 2. Schematic circuit of differential signal recovery.

The input voltages of the instrumentation amplifier can be written as

$$\dot{U}_{-IN} = \dot{U}_0 - \dot{U}_0 K_f; \quad \dot{U}_{+IN} = \dot{U}_X - \dot{U}_0 K_f, \tag{1}$$

where U_X and U_0 are the voltages to be compared, V_f and K_f is the complex transfer factor of the voltage follower.

The output voltage of the instrumentation amplifier relative to the GND_f is as follows:

$$\dot{U}_{OUT} = \dot{K}_d \left(\dot{U}_X - \dot{U}_0 + (\dot{U}_X + \dot{U}_0) / 2 \dot{K}_{CMRR} - \dot{U}_0 \dot{K}_f / \dot{K}_{CMRR} \right) \quad (2)$$

In the case of $U_X \cos(\omega t) = U_0 \cos(\omega t)$, the modulus and the voltage phase at the IA output with the voltage follower connection are determined by the following relations:

$$|U_{OUT}| = \sqrt{U_0^2 \frac{1 - 2K_f \cos \varphi_f + K_f^2}{K_{CMRR}^2}}; \quad \varphi_{OUT} = \arctg\left(\frac{-K_f \sin \varphi_f}{1 - K_f \cos \varphi_f}\right) \quad (3)$$

Therefore, the common-mode rejection ratio directly depends on the accuracy of the complex transfer factor of the voltage follower.

The voltage follower output stage with embedded photovoltaic modules is designed to implement the voltage follower circuit in practice (see Figure 3). These photovoltaic modules are the solar cell array, which generates constant voltage when exposed to light.

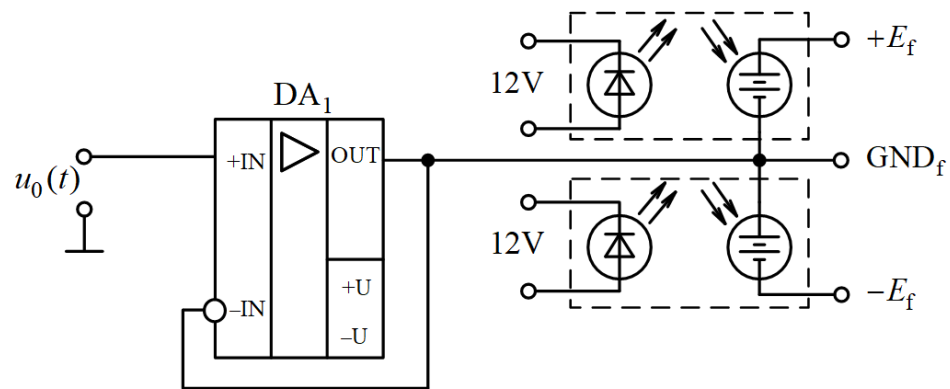


Figure 3. Voltage follower output stage with embedded photovoltaic modules.

The circuit simulation is performed in the NI Multisim simulation program based on an OP285 operating amplifier and photovoltaic modules with 5.6 V design output voltage and 1 W maximum power. Photovoltaic modules are connected to create constant symmetrical voltage $\pm E_f$ when exposed to the light-emitting diode array with the IA quasi-GND for the instrumental amplifier, which is formed by the voltage follower and named GND_f . The light-emitting diode array is supplied by a single constant voltage source $E1$, not connected galvanically to the voltage follower circuit.

In Figure 4, NI Multisim is used to simulate the amplitude frequency and phase-shift-frequency responses of the voltage follower output stage with embedded photovoltaic modules.

Based on (3) and the simulation of $U_X \cos(\omega t) = U_0 \cos(\omega t)$ common-mode signals with 10 V amplitude, we obtain the frequency dependence presented in Figure 5 for the standard PGA207 instrumental amplifier with the design 100 dB CMRR and a 20 dB decrease per decade of ≈ 5 kHz [48]. According to Figure 5, the CMRR increases by 80 dB resulting in 180 dB on a 1 kHz frequency.

SunPower flexible monocrystalline solar cells C60 (Xuancheng, Anhui, China), a voltage follower based on OP285 operating amplifier and a PGA207 instrumental amplifier are used to assemble the prototype of the differential signal recovery as illustrated in Figure 6.

The CMRR is experimentally detected in the prototype of the differential signal recovery by using the circuit shown in Figure 7.

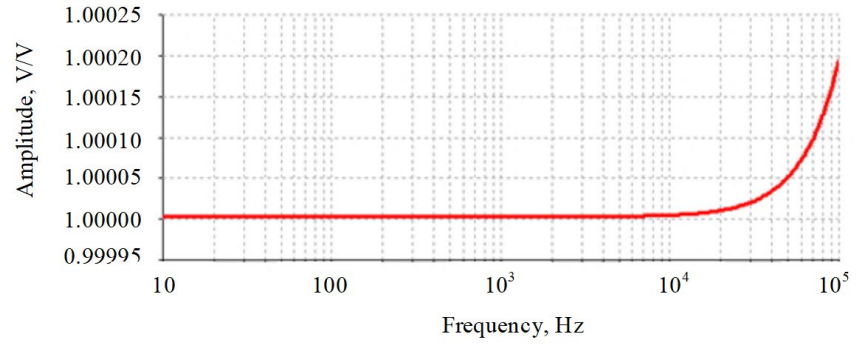
Both inputs of the differential signal recovery are supplied by a Fluke 5520 calibrator with 1, 5 and 10 V sinusoidal voltage $u_0(t)$ on frequencies of 20, 40, 80 and 400 Hz and 1, 10, 20, 40, 80 and 100 kHz. The output voltage of the transformer is measured by an SR830 lock-in amplifier. The IA gain is 10, and the transfer factor of the transformer is 2.

The CMRR can be obtained from

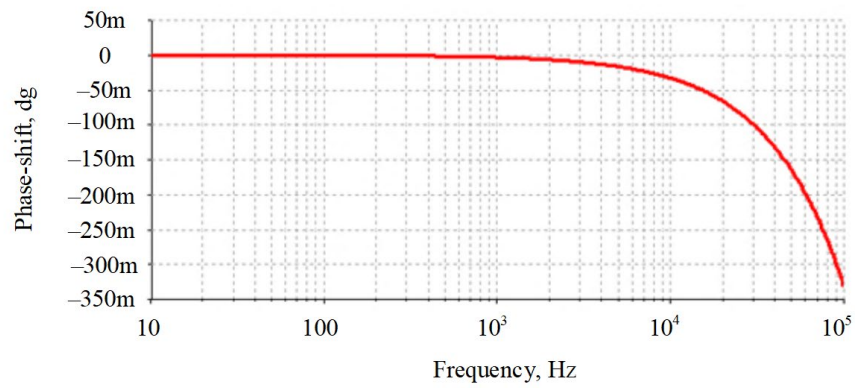
$$K_{CMRR} = 20 \cdot \lg(U_C \cdot K_{IA} \cdot K_T / \Delta U), \tag{4}$$

where U_C is the input common mode voltage, V; K_{IA} is the IA gain; and K_T is the transfer factor of the transformer.

The experimental results are given in Table 2.



(a)



(b)

Figure 4. Amplitude frequency (a) and phase-shift-frequency (b) responses of the IA voltage follower output stage with embedded photovoltaic modules.

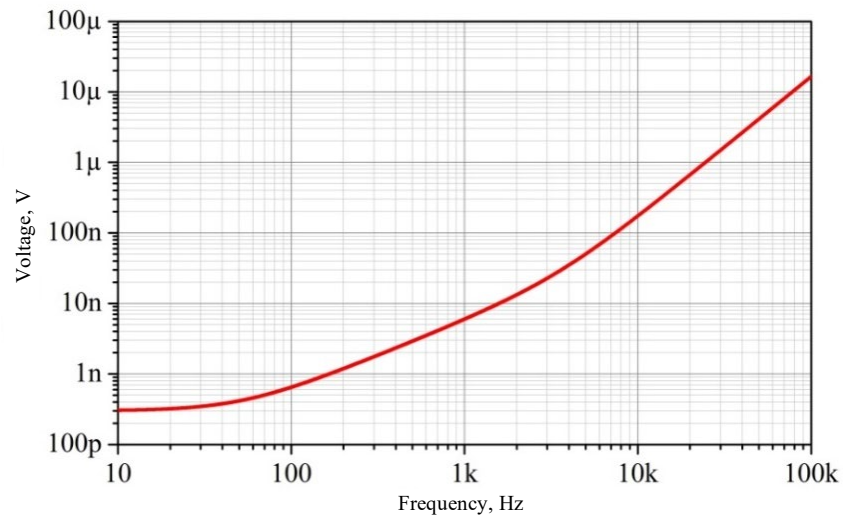


Figure 5. The PGA207 output voltage with the voltage follower output stage with embedded solar cells.

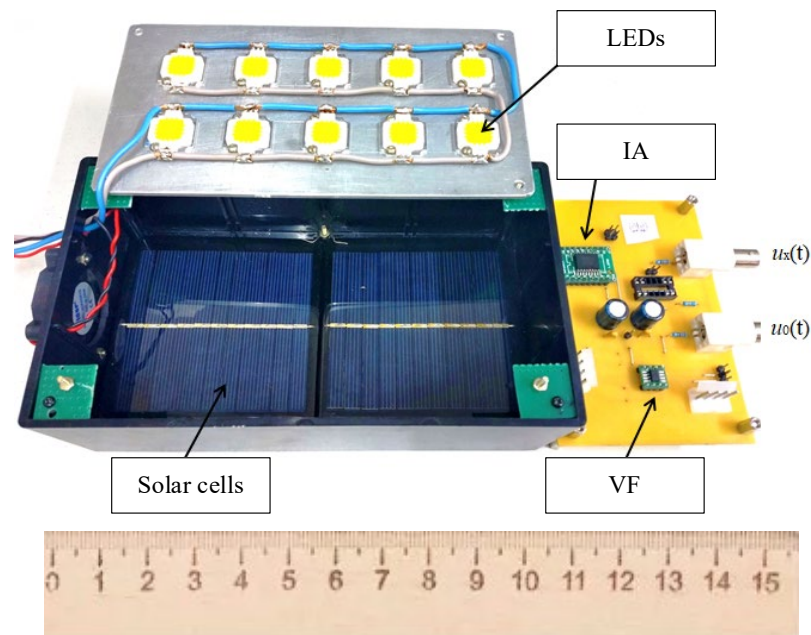


Figure 6. Prototype of differential signal recovery.

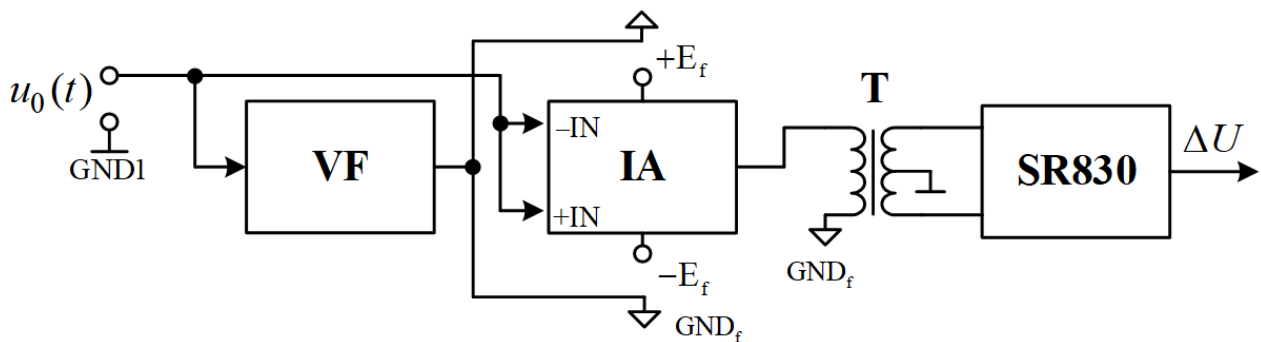


Figure 7. Schematic circuit of CMRR detection in the prototype of differential signal recovery.

Table 2. CMRR values for the differential signal recovery.

Frequency, kHz	CMRR, dB		
	$U_C = 1\text{ V}$	$U_C = 5\text{ V}$	$U_C = 10\text{ V}$
0.02	175.92	176.77	184.08
0.04	175.92	176.42	182.56
0.08	172.04	171.80	176.17
0.4	164.81	163.92	166.83
1	159.79	157.75	158.53
10	133.91	133.80	133.88
20	123.05	122.99	123.07
40	111.38	111.40	111.55
80	99.52	99.51	99.73
100	95.67	95.67	95.81

As presented in Table 2, the implemented circuit of the IA voltage follower output stage with embedded photovoltaic modules provides an 80 dB increase in the CMRR, i.e., up to 100–180 dB in the frequency range up to 100 kHz. This proves the achieved quasi-invariance to the common-mode signal in this frequency range.

4. Lock-In Amplifier with Increased CMRR

Based on the proposed signal recovery, we developed the dual phase lock-in amplifier with the differential input for checking the suggested circuit solution in a real device. The flowchart of the dual phase analog lock-in amplifier is presented in Figure 8.

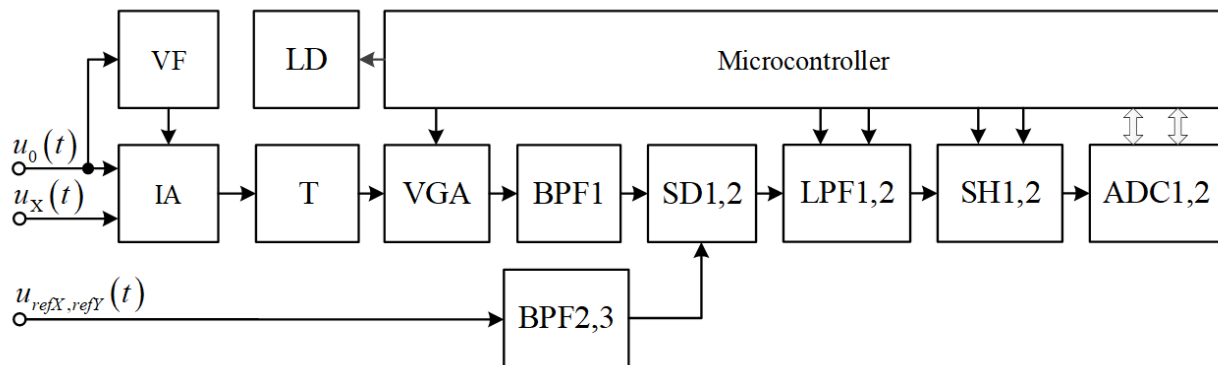


Figure 8. Flowchart of the dual phase analog lock-in amplifier.

According to Figure 8, the lock-in amplifier consists of the input IA with the voltage follower VF (see Figures 2 and 3); isolating transformer T, which has one primary coil with 100 turns and two secondary coils with 100 turns each, with the common midpoint; the three-stage voltage amplifier VGA comprising three in-series IAs PGA207; the two-stage bandpass filters BPF1, BPF2 and BPF3. The first stage is a second-order Bessel high-pass filter with a 0.1 Hz cutoff frequency, and the second is a second-order Bessel low-pass filter with a 4 MHz cutoff frequency.

The filters are assembled in a OP285 operating amplifier. The lock-in amplifier also includes synchronous detectors SD1 and SD2 mounted to AD734 with the denomination factor close to unity; low-pass filters LPF1 and LPF2 are fabricated on the OP285 operating amplifier according to the third-order Bessel filter with a 0.1 Hz cutoff frequency; sample-and-hold circuits SH1 and SH2 made as described in [49]; MAX110 analog-to-digital converters ADC1 and ADC2; a STM32F103 microcontroller; and indicator LD, which is a four-digit seven-segment LED module.

The comparable voltages are supplied to the IA differential inputs. The differential voltage $\Delta u(t)$ at the IA output is supplied to the programmable three-stage voltage amplifier VGA via the isolating transformer T. The VGA output voltage is filtered by the two-stage bandpass filter BPF1. The BPF1 output voltage is supplied to the first inputs of the synchronous detectors SD1 and SD2. Reference in-phase and quadrature voltages are supplied to the second inputs of the SD1 and SD2 via two-stage bandpass filters BPF2 and BPF3. Voltages from SD1 and SD2 are filtered by low-pass filters and digitalized in analog-to-digital converters. The module and phase of the differential voltage are then calculated in a STM32F103 microcontroller. The resulting value is displayed by the indicator LD.

The flowchart of the dual phase analog lock-in amplifier implies the calibration of instrumentation channels. For this purpose, sample-and-hold circuits SH1 and SH2 are used. During calibration, both IA inputs are supplied by the standard voltage $u_0(t)$, sample-and-hold circuits being in a sample mode. Then, zero adjustment is performed through the SH transfer to the hold mode, and the indicator readouts are zeroed.

The microcontroller is also used to control the gain of the programmable amplifier, low-pass filters and sample-and-hold circuits operating modes. The external view of the PCB after mounting of the developed lock-in amplifier is presented in Figure 9. The output voltage module of the lock-in amplifier can be obtained from

$$\Delta U = \frac{\sqrt{u_C^2 + u_Q^2}}{K_{IA} K_T K_{VGA} K_{LPF} U_{ref}}, \quad (5)$$

where U_C and U_Q are the in-phase and quadrature signals at the outputs of the LPF1 and LPF2, respectively; K_{IA} is the design gain 10 of the IA subtraction circuit; K_T is the transfer factor 2 of the isolating transformer T; K_{VGA} is the design gain of 1, 10, 100 and 1000 of the three-stage voltage amplifier VGA; K_{LPF} is the design gain of 1 and 10 of the low-pass filters; and U_{ref} is the reference voltage.

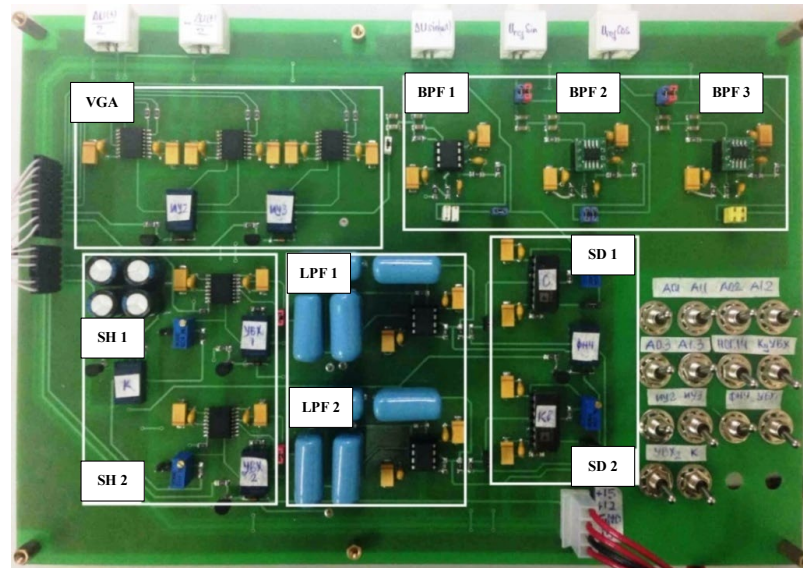


Figure 9. External view of the PCB of the developed lock-in amplifier model.

4.1. CMRR Estimation in Lock-In Amplifier

The CMRR of the lock-in amplifier was measured as follows. The signal generator OWON AG1022 was used to supply voltage $u_0(t)$ $5\sqrt{2}$ V on 20, 40, 80 and 400 Hz and 1, 10, 20, 40, 80 and 100 kHz frequencies from the channel CHA to both inputs of the lock-in amplifier. The channel CHA output was connected to the in-phase reference signal input. From the channel CHB, the quadrature reference signal input was supplied by the voltage of the same amplitude and frequency but with a 90-degree phase shift. The output voltage ΔU was measured, while the CMRR was calculated from

$$K_{CMRR} = 20 \lg \frac{u_0(t)}{\Delta U}. \tag{6}$$

The resulting values of the CMRR with and without sample-and-hold circuits are summarized in Table 3. As can be seen from Table 3, the CMRR of the lock-in amplifier with the sample-and-hold circuit varies from 133 to 180 dB at a frequency of not over 100 kHz.

Table 3. CMRR of the lock-in amplifier.

Frequency, kHz	No Sample-and-Hold		with Sample-and-Hold	
	ΔU , V	K_{CMRR} , dB	ΔU , V	K_{CMRR} , dB
0.02	96×10^{-9}	154.33	$<5 \times 10^{-9}$	>180
0.04	102×10^{-9}	153.81	$<5 \times 10^{-9}$	>180
0.08	103×10^{-9}	153.72	$<5 \times 10^{-9}$	>180
0.4	102×10^{-9}	152.81	$<5 \times 10^{-9}$	>180
1	105×10^{-9}	153.56	6×10^{-9}	178.42
10	1.68×10^{-6}	129.47	26×10^{-9}	165.68
20	5.12×10^{-6}	119.79	80×10^{-9}	155.92
40	21.76×10^{-6}	107.23	235×10^{-9}	146.56
80	82.16×10^{-6}	95.69	612×10^{-9}	138.24
100	130.43×10^{-6}	91.67	1.02×10^{-6}	133.81

4.2. Noise Single Component

The measurement of the noise signal component of the lock-in amplifier was based on the Allan variance at the differential voltage of 1 μV at 1 kHz at the output of the inductive voltage divider DI-3m [50]. The output voltage of the lock-in amplifier was measured for 1 h without using the sample-and-hold circuits. The number of measurements was 720,000.

Figure 10 presents the Allan variance of the lock-in amplifier on a logarithmic scale obtained after the output voltage measurements. A random walk of the output voltage is characterized by the white noise spectrum, and its coefficient is calculated by using the Allan variance at $-1/2$ inclination within the respective time range:

$$N = \sqrt{\sigma(\tau)^2 \cdot \tau} = \sqrt{(6.3 \cdot 10^{-9})^2 \cdot 10}. \tag{7}$$

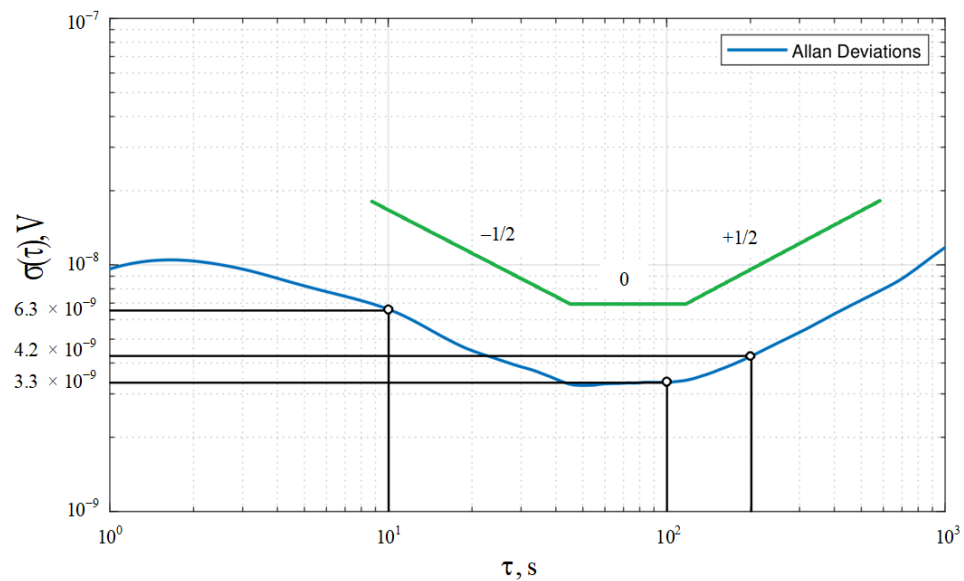


Figure 10. Allan variance of the lock-in amplifier.

The white noise is, thus, 20 nV/ $\sqrt{\text{Hz}}$.

The flicker noise appeared during long-term measurements, which resulted from the electronic parts susceptible to random flickering. Due to its low frequency, the flicker noise was indicated as the data offset fluctuation. Knowing the Allan variance (at a zero inclination), its coefficient was determined as

$$B = \sqrt{\frac{\sigma(\tau)^2 \cdot \pi}{2 \cdot \ln 2}} = \sqrt{\frac{(3.3 \cdot 10^{-9})^2 \cdot \pi}{2 \cdot \ln 2}} \tag{8}$$

and, thus, equal to 5 nV.

The random walk rate was described by the brown noise spectrum at the lock-in amplifier output, while its coefficient was calculated using the Allan variance at $1/2$ inclination within the respective time range:

$$K = \sqrt{\frac{3 \cdot \sigma(\tau)^2}{\tau}} = \sqrt{\frac{3 \cdot (4.2 \cdot 10^{-9})^2}{200}}. \tag{9}$$

The brown noise is, thus, 0.5 nV $\cdot\sqrt{\text{Hz}}$.

The white noise level at the lock-in amplifier output was determined by multiplying the obtained value of the white noise by the square root of the transition band of the low-frequency filter:

$$U_{N.OUT} = N \cdot \sqrt{f_{LPF}} = 20 \cdot 10^{-9} \cdot \sqrt{0.2}. \tag{10}$$

The white noise level is 9 nV.

4.3. Resolution of Lock-In Amplifier

The resolution of the lock-in amplifier was measured in accordance with the circuit presented in Figure 11.

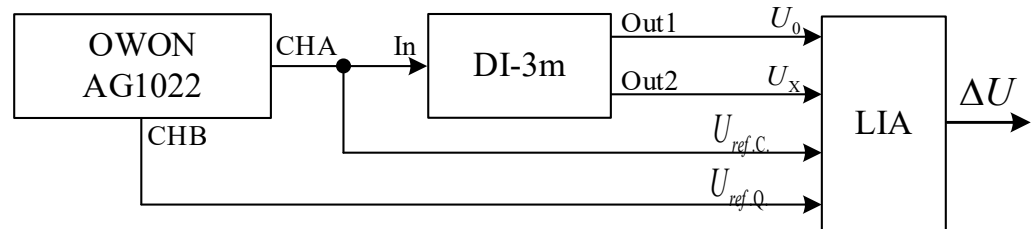


Figure 11. Flowchart of resolution estimation of the lock-in amplifier.

The $1\sqrt{2}$ V output voltage at 1 kHz was supplied from the channel CHA of the signal generator OWON AG1022. The same voltage was supplied from the channel CHB but with a 90-degree phase shift.

According to Figure 11, at output 1, the transfer factor of the voltage divider DI-3 m [50] was 0.500000, whereas at output 2, it varied from 0.500010 to 0.500050.

The relative deviation in measurements is calculated from

$$\gamma = \frac{|(U_{DI} - \Delta U)|}{U_{DI}} \cdot 100\%, \tag{11}$$

where U_{DI} is the differential voltage at the DI-3m outputs, V; and ΔU is the output voltage of the lock-in amplifier, V.

At resolutions of 1 and 100 nV, the lock-in amplifier gain was determined as 2000 ($K_{LIA} = K_{IA} \cdot K_T \cdot K_{VGA} \cdot K_{LPF} = 10 \times 2 \times 100 \times 1 = 2000$). At a resolution of 10 nV, this factor was 20,000 ($K_{LIA} = K_{IA} \cdot K_T \cdot K_{VGA} \cdot K_{LPF} = 10 \times 2 \times 100 \times 10 = 20,000$). The resolution values obtained for the lock-in amplifier using the voltage follower output stage with embedded photovoltaic modules are given in Table 4.

Table 4. Differential voltage at 100 and 10 nV resolutions.

$U_{DI}, \mu V$	100 nV Resolution			10 nV Resolution		
	$\Delta U, \mu V$	$\gamma, \%$	RMS Deviation, %	$\Delta U, \mu V$	$\gamma, \%$	RMS Deviation, %
10	10.1	1.20	0.45	10.11	1.06	0.21
20	20.1	0.30	0.27	20.25	1.24	0.23
30	30.1	0.20	0.18	30.41	1.38	0.13
40	40.1	0.25	0.18	40.54	1.36	0.15
50	50.2	0.32	0.11	50.69	1.38	0.23

As can be seen from Table 4, the relative error of the lock-in amplifier at a 10 and 100 nV resolution does not exceed 1.4% and 1.2%, respectively.

4.4. Frequency Range of Lock-In Amplifier

The estimation of the frequency range of compared voltages was performed by using the flowchart in Figure 11. The output voltage $5\sqrt{2}$ and $0.1\sqrt{2}$ V at 1 kHz was supplied from the channel CHA of the signal generator OWON AG1022, and the same voltage was supplied from the CHB channel but with a 90-degree phase shift.

The transfer factor of the inductive voltage divider DI-3m was 0.100000 at output 1 and 0.100010 at output 2, i.e., the differential input voltage of the lock-in amplifier was 50 μV at $5\sqrt{2}$ V from the signal generator OWON AG1022. The differential voltage was measured at

100 nV resolution on frequencies of 20, 40, 80 and 400 Hz and 1, 10, 20, 40, 80 and 100 kHz. The relative deviation in measurements at different frequencies is calculated from

$$\gamma_f = \frac{|\Delta U_{f=1\text{Hz}} - \Delta U_f|}{\Delta U_{f=1\text{Hz}}} \cdot 100\%, \tag{12}$$

where $\Delta U_{f=1\text{ Hz}}$ is the output voltage of lock-in amplifier on 1 kHz frequency, V; ΔU_f is the output voltage of lock-in amplifier on frequency different from 1 kHz.

The gain of the lock-in amplifier was 2000 and 20,000 for compared voltages of $0.5\sqrt{2}$ and $0.01\sqrt{2}$ V, respectively. The frequency values determined for the compared voltages using the flowchart given in Figure 11 are presented in Table 5.

Table 5. Frequency range of lock-in amplifier.

Frequency, kHz	0.5√2 V		0.01√2 V	
	ΔU _f , μV	γ, %	ΔU _f , μV	γ, %
0.02	49.0	3.5	49.1	3.5
0.04	50.1	1.4	50.3	1.2
0.08	50.4	0.8	50.7	0.4
0.4	50.8	0	50.9	0
1	50.8	–	50.9	–
10	49.3	3.0	49.6	2.6
20	49.9	1.8	50.2	1.4
40	50.5	0.6	50.5	0.8
80	51.5	1.4	50.8	0.2
100	52.1	2.6	50.6	0.6

According to this table, the relative deviation is not over 3.5% in the operating frequency range.

4.5. Minimum and Maximum Amplitudes of Voltages Compared

The estimation of the minimum amplitude of compared voltages was performed by using the flowchart in Figure 11. The output voltage of $1\sqrt{2}$ V at 1 kHz was supplied from the channel CHA of the signal generator OWON AG1022, and the same voltage but with a 90-degree phase shift was supplied from the CHB channel.

The transfer factor of the inductive voltage divider DI-3m was 0.000000 at output 1 and 0.000010 to 0.000050 at output 2, i.e., the differential voltage measured by the lock-in amplifier was varied from 10 to 50 μV. The minimum amplitude measurement of the compared voltage was conducted at a 100 nV resolution and 20,000 gain of the lock-in amplifier. The relative deviation in measurements was calculated by (11). The flowchart of the maximum amplitude of the compared voltages is given in Figure 12.

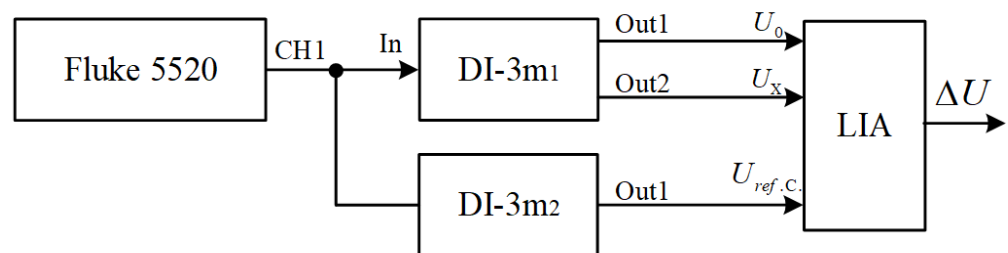


Figure 12. Flowchart of the maximum amplitude of the compared voltages.

The output voltage of $10\sqrt{2}$ V and 1 kHz was supplied from the Fluke 5520 calibrator. The transfer factor of the first voltage divider DI-3₁ was 1.000000 at output 1 and 0.999999 at output 2. The transfer factor of the first voltage divider DI-3₁ at output 2 was changed

from 0.999999 to 0.999995. The reference voltage was supplied from output 1 of the second voltage divider DI-3₂; the transfer factor was 0.500000.

The minimum and maximum amplitudes of the compared voltages are presented in Table 6.

Table 6. Minimum and maximum amplitudes of the compared voltages.

$U_{DI}, \mu V$	Minimum Voltage Amplitudes			Maximum Voltage Amplitudes		
	$\Delta U, \mu V$	$\gamma, \%$	RMS Deviation, %	$\Delta U, \mu V$	$\gamma, \%$	RMS Deviation, %
10	10.2	1.80	0.45	10.2	1.60	0.55
20	20.4	1.90	0.22	20.3	1.60	0.42
30	30.5	1.80	0.30	30.5	1.80	0.87
40	40.7	1.75	0.18	41.0	2.60	0.29
50	50.9	1.84	0.17	51.3	2.68	0.64

According to this table, the dynamic range RMS deviation of the compared voltages is not over 2.68%. This paper clearly shows that the definite metrological parameters of the proposed dual phase analog lock-in amplifier with differential input prove its applicability in comparing two signal amplitudes of $10\sqrt{2} \mu V$ to $10\sqrt{2} V$ in the frequency range of 20 Hz to 100 kHz with a 10 nV resolution and 180 dB common-mode signal.

Table 7 presents specifications for different models of commercially available lock-in amplifiers and our dual phase analog lock-in amplifier.

Table 7. Comparison of commercially-available lock-in amplifiers and our lock-in amplifier.

Models	Price, USD	Max Input Voltage, V	Resolution, nV	Frequency Range, kHz	CMRR, dB
SR830, Stanford Research Systems	4000	1	2	1×10^{-6} –102	100 (≤ 10 kHz)
SR860, Stanford Research Systems	6495	1	1	1×10^{-6} –500	90 (≤ 1 kHz)
SR865A, Stanford Research Systems	7950	1	1	1×10^{-6} –4000	>90 (≤ 1 kHz)
7260, EG&G Instruments	3250	1	2	1×10^{-6} –250	100 (1 kHz)
LI5640, NF Electronic Instruments	2100	1	2	1×10^{-6} –100	120 (1 kHz)
7265, Signal Recovery	4000	1	2	1×10^{-6} –250	>100 (1 kHz)
7230, Signal Recovery	3390	1	10	1×10^{-6} –120	>100 (1 kHz)
MFLI, Zurich Instruments	5200	3	1	DC–500	100 (1 kHz)
Our lock-in amplifier	2500	15	10	20×10^{-3} –100	>180 (1 kHz)

5. Conclusions

In this paper, we presented a developed differential signal recovery circuit with embedded photovoltaic modules and a dual phase lock-in amplifier with a differential input and quasi-invariant common-mode signal.

The embedded photovoltaic modules of the voltage follower in the signal recovery and the sample-and-hold circuit in the measurement channel of the lock-in amplifier allowed increasing the CMRR by 80 dB in the frequency range up to 100 kHz, which proved the gain in the quasi-invariant common-mode signal within that frequency range.

The proposed dual phase analog lock-in amplifier was characterized by a 130 to 185 dB CMRR in the frequency range up to 100 kHz, 20 nV/ \sqrt{Hz} white noise calculated by the Allan variance, the resolution, the frequency range of the compared voltages and their dynamic range.

The obtained metrological parameters of the proposed dual phase analog lock-in amplifier proved their applicability in comparing two signal amplitudes of $10\sqrt{2} \mu V$ to $10\sqrt{2} V$ in the frequency range of 20 Hz to 100 kHz with a 10 nV resolution.

Future works should consider the substitution of analog synchronous detectors, band-pass filters, low-frequency filters and sample-and-hold circuits for their digital equivalents with the purpose to design a digital lock-in amplifier and further improve the metrological parameters based on digital signal processing.

Author Contributions: Conceptualization, P.B.; methodology, P.B.; investigation, I.Z. and B.B.D.; resources, P.B. and B.B.D.; writing—original draft preparation, I.Z.; writing—review and editing, P.B.; visualization, B.B.D. All authors have read and agreed to the published version of the manuscript.

Funding: This work was funded by Grant RSF N 21-79-00083 and carried out within the framework of the Competitiveness Enhancement Program of National Research Tomsk Polytechnic University.

Data Availability Statement: Data about commercially available lock-in amplifiers are available from [27–33].

Conflicts of Interest: The authors declare no conflict of interest.

References

1. Callegaro, L.; D’Elia, V. Guarded vector voltmeter for AC ratio standard calibration. *IEEE Trans. Instrum. Meas.* **2002**, *51*, 632–635. [[CrossRef](#)]
2. Callegaro, L.; Bosco, G.; D’Elia, V.; Serazio, D. Direct-reading absolute calibration of ac voltage ratio standards. *IEEE Trans. Instrum. Meas.* **2003**, *52*, 380–383. [[CrossRef](#)]
3. Corminboeuf, D.; Overney, F. Inductive voltage divider calibration with sampling method. *EPJ Web Conf.* **2014**, *77*, 00014. [[CrossRef](#)]
4. Silveira, F.A. Bootstrap Calibration of Inductive Voltage Dividers at Inmetro. Instrumentation and Detectors. *arXiv* **2019**, arXiv:1904.08759. [[CrossRef](#)]
5. Kon, S.; Yamada, T. AC shunt calibration using a current-bridge method and its validation. *IEEJ Trans. Electr. Electron. Eng.* **2014**, *9*, 577–580. [[CrossRef](#)]
6. So, E.; Angelo, D.; Tsuchiyama, T.; Tadokoro, T.; Waltrip, B.C.; Nelson, T.L. Intercomparison of Calibration Systems for AC Shunts Up to Audio Frequencies. *IEEE Trans. Instrum. Meas.* **2005**, *54*, 507–511. [[CrossRef](#)]
7. Filipski, P.; Boecker, M. AC–DC Current Shunts and System for Extended Current and Frequency Ranges. *IEEE Trans. Instrum. Meas.* **2006**, *55*, 1222–1227. [[CrossRef](#)]
8. Draxler, K.; Styblikova, R. Use of a lock-in amplifier for calibrating an instrument current transformer. In Proceedings of the 2014 IEEE International Instrumentation and Measurement Technology Conference (I2MTC), Montevideo, Uruguay, 12–15 May 2014. [[CrossRef](#)]
9. Draxler, K.; Styblikova, R. Calibration of instrument current transformers at low currents using lock-in amplifier. Presented at the International Conference on Applied Electronics, Pilsen, Czech Republic, 5–6 September 2017. [[CrossRef](#)]
10. Hagen, T.; Budovsky, I.; Benz, S.P.; Burroughs, C.J. Calibration system for AC measurement standards using a pulse-driven Josephson voltage standard and an inductive voltage divider. In Proceedings of the 2012 Conference on Precision electromagnetic Measurements, Washington, DC, USA, 1–6 July 2012. [[CrossRef](#)]
11. Georgakopoulos, D.; Budovsky, I.; Benz, S.P. AC Voltage Measurements to 120 V With a Josephson Arbitrary Waveform Synthesizer and an Inductive Voltage Divider. *IEEE Trans. Instrum. Meas.* **2018**, *68*, 1935–1940. [[CrossRef](#)]
12. Liu, Z.; Zhu, L.; Koffman, A.; Waltrip, B.C.; Wang, Y. Digital lock-in amplifier for precision audio frequency bridge. In Proceedings of the CPEM Digest (Conference on Precision Electromagnetic Measurements), Washington, DC, USA, 1–6 July 2012. [[CrossRef](#)]
13. Huang, L.; Wang, Z.; Yang, Y.; Gao, Y.; Lu, Z. Fundamental comparison measurement between sinusoidal and stepwise-approximated sine wave generated by programmable Josephson voltage standard at NIM. In Proceedings of the CPEM Digest (Conference on Precision Electromagnetic Measurements), Rio de Janeiro, Brazil, 24–29 August 2014. [[CrossRef](#)]
14. Trusov, A.A.; Shkel, A.M. Capacitive detection in resonant MEMS with arbitrary amplitude of motion. *J. Micromech. Microeng.* **2007**, *17*, 1583–1592. [[CrossRef](#)]
15. Cui, J.; Chi, X.Z.; Ding, H.T.; Lin, L.T.; Yang, Z.C.; Yan, G.Z. Transient response and stability of the AGC-PI closed-loop controlled MEMS vibratory gyroscopes. *J. Micromech. Microeng.* **2009**, *19*, 125015. [[CrossRef](#)]
16. Leland, R. Adaptive control of a MEMS gyroscope using Lyapunov methods. *IEEE Trans. Control Syst. Technol.* **2006**, *14*, 278–283. [[CrossRef](#)]
17. Barrios, M.L.R.; Montero, F.E.H.; Mancilla, J.C.G.; Marín, E.P. Application of Lock-In Amplifier on gear diagnosis. *Measurement* **2017**, *107*, 120–127. [[CrossRef](#)]
18. Li, G.; Zhou, M.; Li, X.-X.; Lin, L. Digital lock-in algorithm and parameter settings in multi-channel sensor signal detection. *Measurement* **2013**, *46*, 2519–2524. [[CrossRef](#)]
19. Ye, W.-L.; Zheng, C.-T.; Cheng, X.-Y.; Wu, F.-P.; Chen, M.-M.; Wang, Y.-D. Mid-infrared ppm-level methane detection device using small-size absorption pool and dual-channel lock-in amplifier. *Infrared Phys. Technol.* **2015**, *71*, 339–346. [[CrossRef](#)]
20. Kao, M.-C.; Pegoraro, A.F.; Kingston, D.M.; Stollow, A.; Kuo, W.-C.; Mercier, P.H.J.; Gogoi, A.; Kao, F.-J.; Ridsdale, A. Direct mineralogical imaging of economic ore and rock samples with multi-modal nonlinear optical microscopy. *Sci. Rep.* **2018**, *8*, 16917. [[CrossRef](#)] [[PubMed](#)]
21. Wang, J.; Wang, Z.; Ji, X.; Liu, J.; Liu, G. A simplified digital lock-in amplifier for the scanning grating spectrometer. *Rev. Sci. Instrum.* **2017**, *88*, 023101. [[CrossRef](#)]

22. Hrdý, R.; Kynclová, H.; Klepáčová, I.; Bartošík, M.; Neužil, P. Portable Lock-in Amplifier-Based Electrochemical Method to Measure an Array of 64 Sensors for Point-of-Care Applications. *Anal. Chem.* **2017**, *89*, 8731–8737. [[CrossRef](#)]
23. Huang, K.; Geng, Y.; Zhang, X.; Chen, D.; Cai, Z.; Wang, M.; Zhu, Z. A Wide-Band Digital Lock-In Amplifier and Its Application in Microfluidic Impedance Measurement. *Sensors* **2019**, *19*, 3519. [[CrossRef](#)]
24. Zhang, Z.; Wang, F.; Yuan, T.; Li, C. Multiple self-mixing interferometry based on lock-in amplifier analysis for vibration measurement. *Opt. Rev.* **2020**, *27*, 313–320. [[CrossRef](#)]
25. Kishore, K.; Akbar, S.A. Evolution of Lock-In Amplifier as Portable Sensor Interface Platform: A Review. *IEEE Sens. J.* **2020**, *20*, 10345–10354. [[CrossRef](#)]
26. Ghaderi, E.; Bahreyni, B. Synchronous Demodulation for Low Noise Measurements. *IEEE Instrum. Meas. Mag.* **2021**, *24*, 72–78. [[CrossRef](#)]
27. *Model SR865A 4MHz DSP Lock-In Amplifier. User's Manual*; Stanford Research Systems: Sunnyvale, CA, USA, 2005.
28. *Model SR830 DSP Lock-In Amplifier. User's Manual*; Stanford Research Systems: Sunnyvale, CA, USA, 2011.
29. *Model SR860 500 kHz DSP Lock-In Amplifier. User's Manual*; Stanford Research Systems: Sunnyvale, CA, USA, 2011.
30. *Model 7260 DSP Lock-In Amplifier. Instruction Manual*; EG&G Instruments Corporation: Dallas, TX, USA, 1998.
31. *Model LI 5640 Multifunction Digital Lock-in Amplifier. Instruction Manual*; NF Corporation: Yokohama, Japan, 2002.
32. *Model 7265 DSP Lock-in Amplifier. Instruction Manual*; Ametek Advanced Measurement Technology: Oak Ridge, TN, USA, 1993.
33. *Model MFLI Lock-in Amplifier 500kHz/5MHz. User Manual*; Zurich Instruments: Zürich, Switzerland, 2015.
34. Sutcliffe, H. Lock-In Amplifiers: Principles and Application. *IEE Proc. G Electron. Circuits Syst.* **1984**, *131*, 134. [[CrossRef](#)]
35. Spears, B.K.; Tuffillaro, N.B. A chaotic lock-in amplifier. *Am. J. Phys.* **2008**, *76*, 213–217. [[CrossRef](#)]
36. Meade, M.L. Advances in lock-in amplifiers. *J. Phys. E Sci. Instrum.* **1982**, *15*, 395–403. [[CrossRef](#)]
37. Leis, J.; Martin, P.; Buttsworth, D. Simplified digital lock-in amplifier algorithm. *Electron. Lett.* **2012**, *48*, 259–261. [[CrossRef](#)]
38. Bhagyajyothi, I.J.; Bhaskar, P.; Parvathi, C.S. Design and development of advanced lock-in amplifier and its application. *Sens. Transducers* **2013**, *153*, 22–28.
39. Lu, J.; Pan, D.-A.; Yang, B.; Qiao, L. Wideband magnetoelectric measurement system with the application of a virtual multi-channel lock-in amplifier. *Meas. Sci. Technol.* **2008**, *19*, 045702. [[CrossRef](#)]
40. Zhang, S.; Li, G.; Lin, L.; Zhao, J. Optimization of a digital lock-in algorithm with a square-wave reference for frequency-divided multi-channel sensor signal detection. *Rev. Sci. Instrum.* **2016**, *87*, 085102. [[CrossRef](#)]
41. Macias-Bobadilla, G.; Rodríguez-Reséndiz, J.; Mota-Valtierra, G.; Soto-Zarazúa, G.; Méndez-Loyola, M.; Garduño-Aparicio, M. Dual-Phase Lock-In Amplifier Based on FPGA for Low-Frequencies Experiments. *Sensors* **2016**, *16*, 379. [[CrossRef](#)]
42. Cifuentes, A.; Marín, E. Implementation of a field programmable gate array-based lock-in amplifier. *Measurement* **2015**, *69*, 31–41. [[CrossRef](#)]
43. Baranov, P.; Tsimbalist, E.; Borikov, V.; Pisarenko, J. Increasing common-mode rejection ratio based on the voltage follower. In Proceedings of the 2016 International Siberian Conference on Control and Communications (SIBCON), Moscow, Russia, 12–14 May 2016; pp. 1–3. [[CrossRef](#)]
44. Gerstenhaber, M.; Tran, C. *Composite Instrumentation Amp Extends CMRR Frequency Range 10X*; Electronic Design: Minneapolis, MI, USA, 2002; Volume 50.
45. Albaugh, N. *The Instrumentation Amplifier Handbook. Including Applications*; Burr-Brown Corporation: Tucson, AZ, USA, 2012.
46. Kitchin, C.; Counts, L. *A Designer's Guide to Instrumentation Amplifiers*, 2nd ed.; Analog Devices: Norwood, MA, USA, 2004.
47. Wurcer, S.; Kitchin, C. *Stacked Amplifiers Lower Noise*; Analog Devices: Norwood, MA, USA, 1982.
48. Baranov, P.; Borikov, V.; Ivanova, V.; Duc, B.B.; Uchaikin, S.; Liu, C.-Y. Lock-in amplifier with a high common-mode rejection ratio in the range of 0.02 to 100 kHz. *Acta IMEKO* **2019**, *8*, 103–110. [[CrossRef](#)]
49. Baranov, P.; Borikov, V.; Tsimbalist, E.; Duc, B.B. Decrease uncertainty of measuring small differential signal against large common-mode signal. *MATEC Web Conf.* **2017**, *102*, 01006. [[CrossRef](#)]
50. Kim, V.L.; Cheburenko, D.S.; Merkulov, S.V. Programmable inductive voltage divider. In Proceedings of the 7th International Forum on Strategic Technology, Tomsk, Russia, 18–21 September 2012. [[CrossRef](#)]